Cancer Research
The Journal of Cancer Research (1916–1930) | The American Journal of Cancer (1931–1940)

AACR American Association for Cancer Research

Spermidine prolongs lifespan and prevents liver fibrosis and hepatocellular carcinoma by activating MAP1S-mediated autophagy

Fei Yue, Wenjiao Li, Jing Zou, et al.

Cancer Res Published OnlineFirst April 6, 2017.

Spermidine prolongs lifespan and prevents liver fibrosis and hepatocellular carcinoma by activating MAP1S-mediated autophagy

Fei Yue[1], Wenjiao Li[1], Jing Zou[1], Xianhan Jiang[1,2], Guibin Xu[1,2], Hai Huang[1] and Leyuan Liu[1,2,3]

[1]Center for Translational Cancer Research, Institute of Biosciences and Technology, Texas A&M University, 2121 W. Holcombe Blvd., Houston, Texas, 77030, USA.

[2]The Fifth Affiliated Hospital of Guangzhou Medical University, Guangzhou, Guangdong Province, 510700, China.

[3]Department of Molecular and Cellular Medicine, College of Medicine, Texas A&M University, College Station, Texas, 77843, USA.

Running Title: Spermidine activates autophagy and suppresses HCC via MAP1S

Keywords: animal models in prevention, biological and biochemical mechanism in prevention, diet and cancer, hepatocellular carcinoma, genome instability, natural products, reactive oxygen and carcinogenesis

Grant support: L. Liu, NCI R01CA142862.

Corresponding author: Leyuan Liu, Center for Translational Cancer Research, Institute of Biosciences and Technology, Texas A&M University, 2121 W. Holcombe Blvd., Houston, Texas, 77030, USA. E-mail: lliu@ibt.tamhsc.edu.

Abstract

Liver fibrosis and hepatocellular carcinoma (HCC) have worldwide impact but continue to lack safe, low cost and effective treatments. In this study, we show how the simple polyamine spermidine can relieve cancer cell defects in autophagy which trigger oxidative stress-induced cell death and promote liver fibrosis and HCC. We found that the autophagic marker protein LC3 interacted with the microtubule-associated protein MAP1S which positively regulated autophagy flux in cells. MAP1S stability was regulated in turn by its interaction with the histone deacetylase HDAC4. Notably, MAP1S-deficient mice exhibited a 20% reduction in median survival and developed severe liver fibrosis and HCC under stress. Wild-type mice or cells treated with spermidine exhibited a relative increase in MAP1S stability and autophagy signaling via depletion of cytosolic HDAC4. Extending recent evidence that orally administered spermidine can extend lifespan in mice, we determined that life extension of up to 25% can be produced by lifelong administration which also reduced liver fibrosis and HCC foci as induced by chemical insults. Genetic investigations established that these observed impacts of oral spermidine administration relied upon MAP1S-mediated autophagy. Our findings offer a preclinical proof of concept for the administration of oral spermidine to prevent liver fibrosis and HCC and potentially extend lifespan.

Introduction

Hepatocellular carcinoma (HCC) is the most common form of liver cancers and has become a serious problem in the US in recent decades (1). Most HCC patients also develop liver cirrhosis caused by liver fibrosis; and liver cirrhosis itself is the most common non-neoplastic cause of mortality among hepatobiliary and digestive diseases in the US (1,2). Currently, only a small portion of HCC cases are diagnosed early enough to be treated by surgical resection or liver transplantation, but general patient prognosis is very poor (3). Otherwise, no effective drug for HCC is available. Although hepatitis B virus (HBV) immunization and antiviral therapy against HBV or hepatitis C virus (HCV) in established patients can reduce HCC risk, their cost-effectiveness for HCC prevention in the general population is unknown. Prescribed medications such as statins, metformin and aspirin have shown chemo-preventive effects for HCC, but each simultaneously exhibits other unintended effects (3). Natural dietary components and phytochemicals consumed by humans over their lifetime provide a great window of opportunity to prevent or change the pathogenic course of the disease in a safer and more cost-effective way.

Autophagy is a major pathway for the degradation of dysfunctional organelles and misfolded or aggregated proteins (4). Autophagy defects trigger oxidative stresses and lysosomal rupture which induce different types of cell death including apoptosis, necrosis and pyroptosis (5,6). Pyroptosis is specifically characterized by the activation of caspase-1 and the release of pro-inflammatory cytokines to cause the death of other cells in the environment (7); and it promotes liver fibrosis (8). Liver fibrosis-induced liver regeneration contributes to tumorigenesis with two key events: the generation of

genome instability by oxidative stress and the propagation of genome instability by active cell division. Although an inhibition of autophagy might promote apoptosis or necrosis to kill cancer cells, the activation of autophagy leads to a suppression of pyroptosis to reduce liver fibrosis and delay or prevent HCC development.

Microtubule-associated protein 1S (MAP1S), previously named as C19ORF5, associates with microtubules stabilized by either chemotherapeutic drug and microtubule stabilizer taxanes or tumor suppressive protein RASSF1A (9,10). The specific accumulation of MAP1S short chain in response to mitotic arresting leads to a collapse of mitochondria on mitotic spindle and causes mitotic cell death (11). As a sequence homologue of the microtubule-associated protein MAP1A and MAP1B, MAP1S similarly interacts with mammalian autophagy marker LC3 (12-14), and bridges autophagy components with microtubules and mitochondria to affect the biogenesis and degradation of autophagosomes and suppress genome instability and diethylnitrosamine (DEN)-induced HCC (14,15). Autophagy defects caused by MAP1S depletion promote oxidative stress, liver sinusoidal dilatation and fibronectin-induced liver fibrosis and reduce mouse lifespans (16). Higher levels of MAP1S in tumor tissues predict longer survivals for human patients suffering from either prostate adenocarcinomas (17) or clear cell renal cell carcinomas (18). MAP1S interacts with HDAC4 through a specific domain, and the inhibition of HDAC4 increases the acetylation and stability of MAP1S and activates autophagy flux to degrade aggregates of mutant huntingtin proteins related to Huntington's disease (19). Thus, increasing the levels of MAP1S in mice may cause the activation of autophagy flux to expand lifespans, reduce liver fibrosis and suppress HCC.

Spermidine, a chemical originally isolated from semen and enriched in wheat germ, grapefruit and soybean, was reported to change protein acetylation to regulate autophagy and promote longevity in multiple model systems (20-23). Spermidine mimicking caloric restriction activates autophagy to enhance chemotherapy-induced inhibition of tumor growth possibly through boosting T cell-mediated immune responses (24). MAP1S is one of the proteins whose acetylation was significantly increased upon the exposure to spermidine (22). We hypothesized that spermidine may prolong lifespans and suppress the development of liver fibrosis and HCC by increasing the levels of MAP1S to activate autophagy flux. Indeed, here we show that spermidine increases the acetylation and stability of MAP1S and activates autophagy flux by depleting cytosolic HDAC4 to reduce the association between MAP1S and HDAC4. Spermidine prolongs lifespans, alleviates carbon tetrachloride (CCl_4)-induced liver fibrosis and suppresses DEN-induced HCC through MAP1S in mice. All the benefits of spermidine depend on the presence of MAP1S and do not show in MAP1S$^{-/-}$ mice.

Materials and Methods

Antibodies, plasmids and other reagents.

Monoclonal antibody against MAP1S (Cat# AG10006) was a gift from Precision Antibody™, A&G Pharmaceutical, Inc., Columbia, Maryland, USA. The siRNAs specific to human HDAC4 (sc-35540) and mouse HDAC4 (sc-35541), and antibodies against β-actin (SC-47778), β-Tubulin (sc-9104), Lamin B (sc-20682) and poly-ubiquitin (sc-8017) were from Santa Cruz Biotechnology. Antibody against human LC3 (NB 100-2331) was from Novus Biologicals. Antibodies against α-SMA (ab-5694) and LAMP2 (ab18528) were from abcam. Antibodies against 14-3-3 (#7413), γ-H2AX (#9718 S), acetylated lysine (#9441), ATG4B (#5299), Bcl-2 (#2870), H2AX (#2595), HDAC4 (#7628), p-HDAC4 (S246, #3443), p-HDAC4 (S632, #3424) and PI3KCIII (#4263) were from Cell Signaling Technology. Antibody against HA-tag (MMS-101P) was from Covance. Antibody against p62 (BML-PW9860) was from Enzo Life Sciences International. Horseradish peroxidase-conjugated secondary antibodies against mouse (#172-1011) and rabbit (#172-1019) were from Bio-Rad. Dihydroethidium hydrochloride (D-1168), Earle's Balanced Salt Solution (EBSS, 14115-063), Fetal Bovine Serum (FBS, 26140), FITC rabbit anti-mouse IgG (A21202), Hanks' Balanced Salt Solution (HBSS, 14170-112), Rhodamine Red-X goat anti-mouse IgG (R6393), TO-PRO®-3 Iodide (T3605) and Trypan Blue (15250-061) were from Invitrogen. RFP-LC3 was a gift from Dr. Mizushima (25). Anti-acetyl lysine antibody (clone 4G12, Agarose-conjugate, 16-272), bafilomycin A1 (BAF, 11707), carbon tetrachloride (CCl_4, 289116), cycloheximide (CHX, C1988), diethylnitrosamine (DEN, 0756), EGTA (E4378), Hydroxyproline Assay Kit (MAK008-1KT), Sirius Red (Direct Red 80, 365548) and spermidine (SPD, S4139) were from

Sigma. Spermidine stock solution (1M) was prepared in sterile distilled water and adjusted to PH 7.4 using hydrochloric acid as reported (20). Other antibodies, siRNAs and reagents were described by Zou et al. (26) and Yue el al. (19). Type IV collagenase (11088874103) was from Roche. Dulbecco's Modified Eagle Medium (DMEM, CM001) was from GenDEPOT. Antibiotics (SV30010) and trypsin (SV30031.01) for cell culture were from Thermo Scientific. The K520R mutation was introduced into the full-length HA-MAP1S using QuikChange II kit from Agilent Technologies.

Animal experiments.

Animal protocols were approved by the Institutional Animal Care and Use Committee, Institute of Biosciences and Technology, Texas A&M University. All animals received humane care according to the criteria outlined in the "Guide for the Care and Use of Laboratory Animals" prepared by the National Academy of Sciences and published by the National Institutes of Health (NIH publication 86-23 revised 1985). Wild-type ($MAP1S^{+/+}$) and MAP1S knockout mice ($MAP1S^{-/-}$) were bred and genotyped as described in detail in our previous publications (16,27).

Cell culture and isolation of primary mouse hepatocytes.

Most cell lines including HeLa, HepG2, human embryonic kidney (HEK)-293T, COS-7 cells, HeLa cells stably expressing ERFP-LC3 (HeLa-RFP-LC3), and mouse embryonic fibroblasts (MEF) that were established as described (27). Those cell lines were obtained from the American Type Culture Collection (Manassas, VA, USA) around 2012, amplified and stored at -80 ^{o}C. They were thawed and sub-cultured in the DMEM

containing 10% FBS and antibiotics for up to ten passages. Since those cell lines were solely used for biochemical and cell biological assays and not for study of cancer-related biological functions, they were not authenticated and not tested for mycoplasma. Primary mouse hepatocytes were isolated from 12-week-old male mice following the protocol as described (28). Mice were anesthetized and laparotomized with a U shape incision. The portal vein was cannulated and the inferior vena cava was sectioned. The liver was simultaneously perfused with EBSS medium containing 0.5 mM EGTA, followed by HBSS medium supplied with 0.3 mg/ml type IV collagenase. After perfusion, the liver was cut out and gently squeezed until most of the hepatocytes got out. The cells were filtered through sterile 70-μm-mesh nylon, washed by centrifugation and re-suspended in the culture media. Cell viability was assessed by Trypan Blue staining and cells were seeded at 1×10^6 in the 60 mm dish.

Assays of the impact of spermidine on autophagy and HDAC4 in mice.

To test the acute effect of spermidine on autophagy in mice, one month-old male wild-type or MAP1S$^{-/-}$ mice were subjected to intraperitoneal injection of a single dose of spermidine of 50 mg/kg body weight as previously reported (22). The liver and other organs of mice including brain, lung and heart were collected 3 hrs later to prepare cell lysates for immunoblot analyses.

Survival analyses of mice and other statistical analyses.

To conduct survival analyses, mice were fed with normal drinking water or water containing 3 mM spermidine and observed to record their survival times when they were

found dead or when they were found to be moribund. The overall survivals and median survivals were analyzed by the Kaplan-Meier method. Cox proportional-hazard analysis with univariate or multivariate method was used to explore the effect of variables on overall survivals. Liver tissues collected from 18-month old mice were either frozen or fixed for either immunoblot analysis or staining with dihydroethidine hydrochloride to measure oxidative stress or with Hematoxylin and Eosin (H&E) to analyze sinusoidal dilatation as we previously reported (16). The intensities of protein bands were quantified using ImageJ software and normalized by the levels of loading control β-Actin. Statistical significance was determined by Student's two-tailed t-test with levels of significance set to ns, not significant, $p>0.05$; *, $p\leq0.05$; **, $P\leq0.01$; and ***, $P\leq0.001$.

Induction of liver fibrosis.

To investigate the impact of spermidine on liver fibrosis, three months-old mice were selected to be intraperitoneally injected with 5 μl (0 or 10% CCl_4 in corn oil)/g body weight twice a week for 1 month to induce liver fibrosis as described (29). During the same period, mice were fed with either normal water or water containing 3 mM spermidine. At the end of experiment, mice were weighted and sacrificed to collect liver tissues. Liver tissue sections were stained with H&E and lesion area of liver were quantified using ImageJ software. Liver fibrosis was visualized by Sirius Red staining and quantified by the contents of hydroxyproline, and levels of α-SMA were analyzed either by immunoblot or immunostaining as we previously reported (16).

Induction of HCC.

To detect the tumor suppressive function of spermidine, 15-day-old male mice were intraperitoneally injected with a single dose of 10 μg/g body weight of DEN dissolved in saline. Mice were allowed to continuously drink either normal water or water containing 3 mM spermidine and sacrificed at 7 months after birth to examine the development of HCC as we previously described (14). Body weights, liver weights, ratios of liver weight to body weight and number of surface tumors were recorded. Liver tissues were frozen or fixed for immunoblotting, immunostaining and H&E staining similarly as we previously described (14,16,30).

Cell transfection, immunoprecipitation, protein stability assay, subcellular fractionation and confocal fluorescent microscopy.

Cell transfection, immunoprecipitation, immunoblot analysis and confocal fluorescent microscopy were performed as previously described (19,26). Heavy membrane pellet, light membrane pellet, and soluble fraction were prepared from HeLa cells as described (10). Protein Lamin B served as a nuclear marker and 14-3-3 and β-tubulin served as cytosolic markers.

Results

Spermidine-induced expansion of mouse lifespans depends on MAP1S.

Spermidine has been shown to increase the lifespans of yeast, nematodes and flies in an autophagy-dependent fashion (20,21). It was later confirmed that mice exposed to spermidine at age of 4 or 18 months exhibited a 10% increase of median survivals (23). Spermidine was shown to enhance the acetylation of MAP1S (22). Acetylation of MAP1S activates autophagy; and MAP1S depletion leads to an elevation in oxidative stress and intensity of sinusoidal dilatation in mouse liver tissues; and wild-type mice live a median lifespan of 28.0 months while MAP1S$^{-/-}$ mice live a median lifespans of 22.4 months (16,19). We reasoned that the impact of spermidine on mouse lifespans may depend on MAP1S. We fed both wild-type and MAP1S$^{-/-}$ mice continuously for 18 months with either normal water or water containing spermidine immediately after they were weaned, and found that spermidine increased the levels of MAP1S protein in wild-type mice (**Fig. 1A,B**). As previously reported, similar increases in both levels of oxidative stress (**Fig. 1C,D**) and intensities of sinusoidal dilatation (**Fig. 1E,F**) and a similar reduction in lifespans (from 26.9 to 21.9 months) were observed when MAP1S was deleted in mice (**Fig. 1G,H**). Spermidine-treated wild-type mice exhibited significantly lower levels of oxidative stress (**Fig. 1C,D**) and lower intensities of sinusoidal dilatation in liver tissues (**Fig. 1E,F**), and a 25% increase of median survival times from the normal 26.9 months of untreated wild-type mice to 33.3 months (**Fig. 1G,H**). Comparing to the reported 10% increase of median survivals in mice treated with spermidine at late stage of life cycle, a significant enhancement of mouse longevity was achieved when mice were exposed to spermidine immediately after weaning. The

elevated oxidative stress, increased intensities of sinusoidal dilatation and reduced lifespans caused by MAP1S deletion were not significantly changed by the spermidine treatment (**Fig. 1C-H**). Thus, the spermidine-induced expansion of lifespans depends on MAP1S.

Spermidine alleviates liver fibrosis through MAP1S.

We reported that MAP1S-activated autophagy promotes the degradation of fibronectin in lysosomes and alleviates stress-induced liver fibrosis (16). We were triggered to examine the impact of spermidine on liver fibrosis in a mouse model. We treated both wild-type and MAP1S$^{-/-}$ mice with CCl_4 and fed them with either normal or spermidine-containing water. We found that CCl_4 did not change the body weights but increased the liver weights and liver/body weight ratios of both wild-type and MAP1S$^{-/-}$ mice; and spermidine exposure helped the wild-type but not the MAP1S$^{-/-}$ mice to counteract the CCl_4-induced increases of liver weights and liver/body weight ratios (**Fig. 2A-D**). Spermidine exposure led to reductions in both liver lesions caused by CCl_4 in wild-type but not in MAP1S$^{-/-}$ mice (**Fig. 2E,F**) and intensities of CCl4-induced liver fibrosis indicated by the conventional Sirius Red staining in wild-type but not in MAP1S$^{-/-}$ mice (**Fig. 2G,H**). The same trends were confirmed by other assays of liver fibrosis such as the contents of hydroxyl-proline (**Fig. 2I**) and levels of a-SMA as revealed by both immunoblotting and immunostaining (**Fig. 2J-M**). Therefore, spermidine exposure leads to an alleviation of liver fibrosis through MAP1S.

Spermidine suppresses HCC through MAP1S.

We previously reported that MAP1S-deficient mice exposed to DEN developed more and larger foci of HCC than the wild-type (14). We predicted that spermidine promotes MAP1S-activated autophagy to suppress HCC. We injected mice with DEN and examined the tumor development in 7-month-old mice. It was confirmed that MAP1S suppressed the development of HCC (**Fig. 3A**). Wild-type mice drinking water containing spermidine after DEN injection exhibited reduced liver weights, liver/body weight ratios and less surface tumors although the body weights were not altered (**Fig. 3A-E**). The typical trabecular structure of HCC as displayed by H&E staining were dramatically reduced (**Fig. 3F**). The levels of MAP1S were significantly elevated to activate autophagy flux so that the levels of total poly-ubiquitinated proteins were significantly reduced (**Fig. 3G-I**), and number of cells with DNA double strand breaks represented by positive γ-H2AX signals were decreased (**Fig. 3J,K**). MAP1S depletion promoted the development of HCC in MAP1S$^{-/-}$ mice while further spermidine exposure exhibited no significant reduction in protein aggregates, DNA damages and HCC (**Fig. 3**). Therefore, suppressive role of spermidine on the development of HCC also acts through MAP1S.

Spermidine-induced activation of autophagy flux depends on MAP1S.

To understand how spermidine impacts on lifespans, liver fibrosis and HCC through MAP1S, we treated HeLa or MEF cells with spermidine and observed increased levels of MAP1S and autophagy marker LC3-II in a time and dosage-dependent way (**Fig. 4A-D**). The levels of LC3-II in the presence of lysosomal inhibitor bafilomycin A1 were elevated upon exposure to spermidine (**Fig. 4E,F**), suggesting that spermidine

accelerated autophagy flux. The spermidine-induced activation of autophagy flux was further confirmed by the accumulation of RFP-LC3 punctate foci in spermidine-treated HeLa cells stably expressing RFP-LC3 in the absence or presence of lysosomal inhibitor (**Fig. 4G,H**). Therefore, spermidine increases the levels of MAP1S and autophagy flux.

Intraperitoneal injection of a single dose of spermidine to wild-type mice led to a similar increase in levels of MAP1S and LC3-II in livers and other organs of mice including brain and heart (**Fig. 4I,J**). The correlation between levels of MAP1S and autophagy flux upon spermidine treatment triggered our interest to investigate their cause-effect relation. The spermidine-induced increases in LC3-II levels were not observed in different organs or MEFs from MAP1S knockout mice (**Fig. 4I-J**). The spermidine-induced increase in autophagy flux as indicated by the levels of LC3-II in the presence of bafilomycin A1 were observed in wild-type but not in MAP1S$^{-/-}$ hepatocytes or MEFs (**Fig. 4M-P**). Therefore, the activation of autophagy flux by spermidine requires the presence of MAP1S.

Spermidine-enhanced acetylation and stability of MAP1S depends on HDAC4.

We reported that HDAC4 directly interacts with MAP1S through a specific domain and acts as a deacetylase of MAP1S. Using purified active, heat-inactive HDAC4, inactive HDAC4 mutant and MAP1S, we confirmed that MAP1S is the substrate of HDAC4 deacetylase in vitro (19). We reasoned that spermidine may increase the levels of MAP1S-mediated autophagy by regulating HDAC4. We found that spermidine treatment resulted in increases in both levels of acetylated MAP1S (**Fig.**

5A-C) and stability of MAP1S protein (**Fig. 5D,E**). We re-confirmed the interaction between HDAC4 and MAP1S in HepG2 cells (**Fig. 5F**). Reducing the levels of HDAC4 with a previously certified HDAC4-specific siRNA (19) led to increases of MAP1S levels, and further treatment of HDAC4-suppressed cells with spermidine did not induce the activation of autophagy flux (**Fig. 5G-I**). Therefore, spermidine enhances acetylation and stability of MAP1S protein to activate autophagy flux through HDAC4.

Spermidine enhances nuclear translocation and cytosolic depletion of HDAC4.

It would be logically plausible if spermidine treatment acted similarly as the HDAC4-speacific siRNA and led to a reduction in HDAC4 levels. However, spermidine treatment led to increases in HDAC4 levels in a dosage and time-dependent way in different cell lines and different organs of mice (**Fig. 5J-N**). Although HDAC4 was overexpressed, spermidine exposure enhanced the nuclear translocation of HDAC4 (**Fig. 5O-R**) and reduced the actual levels of cytosolic HDAC4 in different types of cells (**Fig. 5S,T**). Therefore, spermidine causes a depletion of cytosolic HDAC4.

Spermidine reduces the interaction of HDAC4 with MAP1S.

Binding of phosphorylated HDAC4 with 14-3-3 keeps both of them stayed in cytosol (31). Spermidine treatment actually significantly reduced the levels of phosphorylated HDAC4 and its binding partner 14-3-3 (**Fig. 6A,B**). The spermidine treatment reduced the interaction of HDAC4 with 14-3-3 (**Fig. 6C,D**), the interaction of HDAC4 with MAP1S (**Fig. 6E-J**) and the colocalization of HDAC4 with MAP1S in

cytosol (**Fig. 6K,L**). Therefore, spermidine treatment decreases the levels of MAP1S-associated HDAC4 although the total levels of HDAC4 is increased.

The spermidine-specific lysine residue 520 of MAP1S is important for MAP1S to promote autophagosomal degradation.

Lysine residue 520 (K520) of human MAP1S was identified in a screen for acetylated sites arising in the presence of spermidine (22). We mutated the lysine residue 520 to arginine (K520R). The K520R mutant of MAP1S protein exhibited higher levels of expression but lower degrees of interaction with HDAC4 than the wild-type (**Fig. 7A**) although it distributed in cytosol similarly to the wild-type (**Fig. 7B**). However, overexpression of the MAP1S mutant resulted in a blockade of autophagosomal degradation and an accumulation of autophagosomes (**Fig. 7C-F**). The forced expression of the K520R mutant at levels higher than the wild-type led to the sustaining levels of autophagosomal biogenesis (**Fig. 7C-F**), suggesting the role of MAP1S in autophagy initiation remained intact despite the mutation. Notably, the amount of punctate foci of RFP-LC3 not associated with LAMP2-labeled lysosomes in cells expressing the MAP1S mutant was higher than in cells expressing wild-type MAP1S (**Fig. 7G,H**). This confirmed that mutation of K520 in MAP1S reduced the efficiency of autophagosome-lysosome fusion, one of the functions of MAP1S in autophagy (27). To further test whether the impact of spermidine on autophagy depends on MAP1S, we re-expressed the wild-type and K520R mutant in MAP1S$^{-/-}$ MEFs. Spermidine-induced activation of autophagy flux was restored in cells expressing the wild-type but not the

K520R mutant (**Fig. 7I,J**). Thus, spermidine-specific lysine residue 520 of MAP1S is important for MAP1S to promote autophagosomal degradation.

Discussion

Polyamines were found in both prokaryotic and eukaryotic systems after initially being identified in human semen in 1678 (32). Difluoromethylornithine (DFMO) is a specific inhibitor of ornithine decarboxylase (ODC), one of the key enzymes involved in biosynthesis of polyamines including spermidine (33). Since spermidine was found to be dramatically elevated in the urine of many cancer patients in 1971 (34), there have been attempts to use the biosynthesis pathway of polyamines as therapeutic target or use levels of polyamines as prognostic markers for cancer patients. DFMO plus sulindac has been shown to effectively prevent the recurrence of colon polyp in a phase III clinical trial (33). Although polyamine depletion has been suggested for cancer prevention, neither alone nor in combination with other agents was DFMO clinically effective (35). Recently, spermidine was shown to activate autophagy flux to prolong lifespans in model systems through promoting convergent deacetylation and acetylation reactions in the cytosol and in the nucleus, respectively (20-22). Although it was claimed that spermidine induces autophagy by inhibiting the acetyltransferase EP300, knockdown of EP300 or inhibition of EP300 by a specific antagonist at concentrations significantly inducing autophagy activation failed to cause a significant decrease of lysine deacetylation of cytosolic proteins (36). The precise biochemical function of spermidine was considered as one of the remaining mysteries of molecular cell biology (35).

In contrast, here we show that spermidine promotes the nuclear translocation of HDAC4 leading to the depletion of cytosolic HDAC4 and a reduction in HDAC4-MAP1S interaction. Spermidine specifically inhibits the deacetylation of the cytosolic autophagy activator MAP1S so that autophagy flux is enhanced. The spermidine-induced activation

of autophagy flux requires the presence of HDAC4 and MAP1S as confirmed in multiple systems. Nuclear translocation of HDAC4 depends on the de-phosphorylation of HDAC4 residue Serine 246 and Serine 632 (37). Immunoblot analysis here shows that the levels of phosphorylated S246 or S632 HDAC4 are significantly reduced upon exposure to spermidine. Therefore, spermidine may promote the de-phosphorylation and nuclear translocation of HDAC4. Further understanding the mechanism by which spermidine promotes de-phosphorylation of HDAC4 is currently undergoing. It was reported that suppression of LKB1-AMPK dramatically reduces levels of phosphorylated HDAC4 (38). Spermidine treatment exhibited no impact on the phosphorylation of mTOR substrate RPS6KB1, or AMPK substrate, acetyl-CoA carboxylase, so that autophagy initiation through the mTOR pathway was not affected (22). It is possible that spermidine only alters the HDAC4-specific activity of LKB1.

Aging is the process that an individual organism becomes older, and characterized by an increasing morbidity and functional decline that eventually result in the death of an organism (39). Caloric restriction, methionine restriction and rapamycin addition were the few interventions that truly prolong the lifespans of vertebrates (40-42). Other interventions such as resveratrol, metformin and sirtuin activators were also reported to extend mouse lifespans (39). However, resveratrol only exhibited effect in mice on high-fat diets (43); metformin slightly increased lifespans when mice were fed with low doses but dramatically reduced the lifespans when mice were fed with high doses (44); and a sirt1 activator had no effect on the maximal lifespans at all (45). Spermidine-related knowledge for cancer patients, spermidine has been reported to reactivate autophagy to ameliorate myopathic defects (46) and prolong the lifespans of

mice (23). Our results show that mice drinking spermidine-containing water immediately after weaning achieve much more significant improvement of lifespans than those start to be treated with spermidine at the age of 4 or 18 months (23). Although they are successful in mouse models, both voluntary caloric restriction and methionine-deficient vegan diet are hard to gain much popularity for general human population, and rapamycin has additional immunosuppressant functions in humans (47). Since spermidine is a natural component originally isolated from semen and plentiful in a variety of food and agricultural products such as wheat germ, grapefruit and Natto (a Japanese product of fermented soy), and can be chemically synthesized and developed as a drink or a dietary supplement to serve with normal diets, it will be a promising safe and cost-effective intervention that will be readily adopted for long-term intervention by the general human population to extend lifespans. Besides, spermidine suppresses liver fibrosis or HCC in mice exposed to a strong chemical inducer of liver fibrosis or a potent chemical carcinogen. Consuming spermidine over the lifetime of humans provide a novel paradigm to prevent, change or reverse the pathogenic course of liver fibrosis and HCC in a safe and cost-effective way for patients with chronic liver diseases or with high risk for developing HCC, and patients already developing HCC. Thus, a great potential impact on human health is anticipated.

Strikingly, all the impacts of spermidine on lifespans, liver fibrosis and HCC depend on the presence of MAP1S, and disappear in the MAP1S knockout mice. Although other function of spermidine may exist, the main functions of spermidine on the expansion of lifespans and suppression of liver fibrosis and HCC are mediated by the MAP1S-activated autophagy. It is well known that manipulation of autophagy flux

through caloric restriction and medication of rapamycin and resveratrol can reduce age-related pathologies and extend longevity (20,36). We recently have reported that MAP1S-activated autophagy is positively related to longevity of mice. MAP1S activates autophagy to suppress oxidative stress and sustain the lifespans of mice expressing high levels of fibronectin. The MAP1S-deficient mice with autophagy defects exhibit much dramatically shortened lifespans in the presence of high levels of fibronectin (16). Here we further indicate that utilizing spermidine to further enhance the MAP1S-activated autophagy flux leads to a dramatic expansion of the lifespans of wild-type mice. Activated autophagy flux results in suppression of oxidative stress, which further leads to suppression of liver fibrosis and HCC. The close association of MAP1S-activated autophagy with survivals of cancer patients further suggest the importance of MAP1S (17,18). Our approach to increase spermidine seems contradicted but actually consistent with the DFMO plus sulindac trial, because it is the nonsteroidal anti-inflammatory drug sulindac that exerts the tumor suppressive function in the clinical trial. Sulindac itself and a derivate of sulindac also inhibit cancer cell growth through induction of autophagy (48-50). Therefore, the characterization of MAP1S-activated autophagy flux in enhancement of longevity and suppression of liver fibrosis and HCC in mice will provide a novel strategy to promote MAP1S-activated autophagy flux to prolong lifespans, to prevent or reverse liver fibrosis, and to prevent, delay or cure HCC in humans.

References

1. El-Serag HB. Hepatocellular carcinoma. New Eng J Med 2011;365(12):1118-27.
2. Zhang DY, Friedman SL. Fibrosis-dependent mechanisms of hepatocarcinogenesis. Hepatology 2012;56(2):769-75.
3. Singh S, Singh PP, Roberts LR, Sanchez W. Chemopreventive strategies in hepatocellular carcinoma. Nat Rev Gastroenterol Hepatol 2014;11(1):45-54.
4. Mizushima N, Noda T, Yoshimori T, Tanaka Y, Ishii T, George MD, et al. A protein conjugation system essential for autophagy. Nature 1998;395(6700):395-8.
5. Fink SL, Cookson BT. Apoptosis, pyroptosis, and necrosis: mechanistic description of dead and dying eukaryotic cells. Infect Immun 2005;73(4):1907-16.
6. Suzuki T, Franchi L, Toma C, Ashida H, Ogawa M, Yoshikawa Y, et al. Differential regulation of caspase-1 activation, pyroptosis, and autophagy via Ipaf and ASC in Shigella-infected macrophages. PLoS Pathog 2007;3(8):e111.
7. Doitsh G, Galloway NL, Geng X, Yang Z, Monroe KM, Zepeda O, et al. Cell death by pyroptosis drives CD4 T-cell depletion in HIV-1 infection. Nature 2014;505(7484):509-14.
8. Wree A, Eguchi A, McGeough MD, Pena CA, Johnson CD, Canbay A, et al. NLRP3 inflammasome activation results in hepatocyte pyroptosis, liver inflammation, and fibrosis in mice. Hepatology 2014;59(3):898-910.
9. Liu L, Vo A, Liu G, McKeehan WL. Distinct structural domains within C19ORF5 support association with stabilized microtubules and mitochondrial aggregation and genome destruction. Can Res 2005;65(10):4191-201.

10. Liu L, Vo A, McKeehan WL. Specificity of the methylation-suppressed A isoform of candidate tumor suppressor RASSF1 for microtubule hyperstabilization is determined by cell death inducer C19ORF5. Can Res 2005;65(5):1830-8.
11. Liu L, Xie R, Yang C, McKeehan WL. Dual function microtubule- and mitochondria-associated proteins mediate mitotic cell death. Cell Oncol 2009;31(5):393-405.
12. Kayaba H, Hirokawa M, Watanabe A, Saitoh N, Changhao C, Yamada Y, et al. Serum markers of graft-versus-host disease after bone marrow transplantation. J Allergy Clin Immunol 2000;106(1 Pt 2):S40-4.
13. Schoenfeld TA, McKerracher L, Obar R, Vallee RB. MAP 1A and MAP 1B are structurally related microtubule associated proteins with distinct developmental patterns in the CNS. J Neurosci 1989;9(5):1712-30.
14. Xie R, Wang F, McKeehan WL, Liu L. Autophagy enhanced by microtubule- and mitochondrion-associated MAP1S suppresses genome instability and hepatocarcinogenesis. Can Res 2011;71(24):7537-46.
15. Liu L, McKeehan WL, Wang F, Xie R. MAP1S enhances autophagy to suppress tumorigenesis. Autophagy 2012;8(2):278-80.
16. Li W, Zou J, Yue F, Song K, Chen Q, McKeehan WL, et al. Defects in MAP1S-mediated autophagy cause reduction in mouse lifespans especially when fibronectin is overexpressed. Aging Cell 2016;15(2):370-9.
17. Jiang X, Zhong W, Huang H, He H, Jiang F, Chen Y, et al. Autophagy defects suggested by low levels of autophagy activator MAP1S and high levels of autophagy inhibitor LRPPRC predict poor prognosis of prostate cancer patients. Mol Carcinog 2015;54(10):1194-204.

18. Xu G, Jiang Y, Xiao Y, Liu XD, Yue F, Li W, et al. Fast clearance of lipid droplets through MAP1S-activated autophagy suppresses clear cell renal cell carcinomas and promotes patient survival. Oncotarget 2016;7(5):6255-65.
19. Yue F, Li W, Zou J, Chen Q, Xu G, Huang H, et al. Blocking the association of HDAC4 with MAP1S accelerates autophagy clearance of mutant Huntingtin. Aging 2015;7(10):839-53.
20. Eisenberg T, Knauer H, Schauer A, Buttner S, Ruckenstuhl C, Carmona-Gutierrez D, et al. Induction of autophagy by spermidine promotes longevity. Nat Cell Biol 2009;11(11):1305-14.
21. Morselli E, Galluzzi L, Kepp O, Criollo A, Maiuri MC, Tavernarakis N, et al. Autophagy mediates pharmacological lifespan extension by spermidine and resveratrol. Aging 2009;1(12):961-70.
22. Morselli E, Marino G, Bennetzen MV, Eisenberg T, Megalou E, Schroeder S, et al. Spermidine and resveratrol induce autophagy by distinct pathways converging on the acetylproteome. J Cell Biol 2011;192(4):615-29.
23. Eisenberg T, Abdellatif M, Schroeder S, Primessnig U, Stekovic S, Pendl T, et al. Cardioprotection and lifespan extension by the natural polyamine spermidine. Nat Med 2016; 22(12):1428-1438.
24. Pietrocola F, Pol J, Vacchelli E, Rao S, Enot DP, Baracco EE, et al. Caloric Restriction Mimetics Enhance Anticancer Immunosurveillance. Can Cell 2016;30(1):147-60.

25. Mizushima N, Yamamoto A, Matsui M, Yoshimori T, Ohsumi Y. In vivo analysis of autophagy in response to nutrient starvation using transgenic mice expressing a fluorescent autophagosome marker. Mol Biol Cell 2004;15(3):1101-11.
26. Zou J, Yue F, Li W, Song K, Jiang X, Yi J, et al. Autophagy inhibitor LRPPRC suppresses mitophagy through interaction with mitophagy initiator Parkin. PloS One 2014;9(4):e94903.
27. Xie R, Nguyen S, McKeehan K, Wang F, McKeehan WL, Liu L. Microtubule-associated protein 1S (MAP1S) bridges autophagic components with microtubules and mitochondria to affect autophagosomal biogenesis and degradation. J Biol Chem 2011;286(12):10367-77.
28. Glick D, Zhang W, Beaton M, Marsboom G, Gruber M, Simon MC, et al. BNip3 regulates mitochondrial function and lipid metabolism in the liver. Mol Cell Biol 2012;32(13):2570-84.
29. Tomita K, Teratani T, Suzuki T, Shimizu M, Sato H, Narimatsu K, et al. Acyl-CoA:cholesterol acyltransferase 1 mediates liver fibrosis by regulating free cholesterol accumulation in hepatic stellate cells. J Hepatol 2014;61(1):98-106.
30. Jiang X, Li X, Huang H, Jiang F, Lin Z, He H, et al. Elevated levels of mitochondrion-associated autophagy inhibitor LRPPRC are associated with poor prognosis in patients with prostate cancer. Cancer 2014;120(8):1228-36.
31. Grozinger CM, Schreiber SL. Regulation of histone deacetylase 4 and 5 and transcriptional activity by 14-3-3-dependent cellular localization. Proc Nat Acad Sci USA 2000;97(14):7835-40.

32. Bachrach U. The early history of polyamine research. Plant Physiol Biochem 2010;48(7):490-5.
33. Meyskens FL, Jr., McLaren CE, Pelot D, Fujikawa-Brooks S, Carpenter PM, Hawk E, et al. Difluoromethylornithine plus sulindac for the prevention of sporadic colorectal adenomas: a randomized placebo-controlled, double-blind trial. Can Prev Res 2008;1(1):32-8.
34. Russell DH. Increased polyamine concentrations in the urine of human cancer patients. Nat New Biol 1971;233(39):144-5.
35. Miller-Fleming L, Olin-Sandoval V, Campbell K, Ralser M. Remaining Mysteries of Molecular Biology: The Role of Polyamines in the Cell. J Mol Biol 2015;427(21):3389-406.
36. Pietrocola F, Lachkar S, Enot DP, Niso-Santano M, Bravo-San Pedro JM, Sica V, et al. Spermidine induces autophagy by inhibiting the acetyltransferase EP300. Cell Death Different 2015;22(3):509-16.
37. Zhao X, Ito A, Kane CD, Liao TS, Bolger TA, Lemrow SM, et al. The modular nature of histone deacetylase HDAC4 confers phosphorylation-dependent intracellular trafficking. J Biol Chem 2001;276(37):35042-8.
38. Mihaylova MM, Vasquez DS, Ravnskjaer K, Denechaud PD, Yu RT, Alvarez JG, et al. Class IIa histone deacetylases are hormone-activated regulators of FOXO and mammalian glucose homeostasis. Cell 2011;145(4):607-21.
39. Mitchell SJ, Scheibye-Knudsen M, Longo DL, de Cabo R. Animal models of aging research: implications for human aging and age-related diseases. Annu Rev Anim Biosci 2015;3:283-303.

40. McCay CM, Maynard LA, Sperling G, Barnes LL. The Journal of Nutrition. Volume 18 July--December, 1939. Pages 1--13. Retarded growth, life span, ultimate body size and age changes in the albino rat after feeding diets restricted in calories. Nutr Rev 1975;33(8):241-3.
41. Orentreich N, Matias JR, DeFelice A, Zimmerman JA. Low methionine ingestion by rats extends life span. J Nutr 1993;123(2):269-74.
42. Harrison DE, Strong R, Sharp ZD, Nelson JF, Astle CM, Flurkey K, et al. Rapamycin fed late in life extends lifespan in genetically heterogeneous mice. Nature 2009;460(7253):392-5.
43. Bauer MA, Carmona-Gutierrez D, Ruckenstuhl C, Reisenbichler A, Megalou EV, Eisenberg T, et al. Spermidine promotes mating and fertilization efficiency in model organisms. Cell Cycle 2013;12(2):346-52.
44. Martin-Montalvo A, Mercken EM, Mitchell SJ, Palacios HH, Mote PL, Scheibye-Knudsen M, et al. Metformin improves healthspan and lifespan in mice. Nat Commun 2013;4:2192.
45. Mitchell SJ, Martin-Montalvo A, Mercken EM, Palacios HH, Ward TM, Abulwerdi G, et al. The SIRT1 activator SRT1720 extends lifespan and improves health of mice fed a standard diet. Cell Rep 2014;6(5):836-43.
46. Chrisam M, Pirozzi M, Castagnaro S, Blaauw B, Polishchuck R, Cecconi F, et al. Reactivation of autophagy by spermidine ameliorates the myopathic defects of collagen VI-null mice. Autophagy 2015: **11**(12):2142-52.
47. Zhang Y, Bokov A, Gelfond J, Soto V, Ikeno Y, Hubbard G, et al. Rapamycin extends life and health in C57BL/6 mice. J Gerontol 2014;69(2):119-30.

48. Gurpinar E, Grizzle WE, Shacka JJ, Mader BJ, Li N, Piazza NA, et al. A novel sulindac derivative inhibits lung adenocarcinoma cell growth through suppression of Akt/mTOR signaling and induction of autophagy. Mol Can Therap 2013;12(5):663-74.

49. Yin T, Wang G, Ye T, Wang Y. Sulindac, a non-steroidal anti-inflammatory drug, mediates breast cancer inhibition as an immune modulator. Sci Rep 2016;6:19534.

50. Chiou SK, Hoa N, Hodges A. Sulindac sulfide induces autophagic death in gastric epithelial cells via survivin down-regulation: a mechanism of NSAIDs-induced gastric injury. Biochem Pharmacol 2011;81(11):1317-23.

FIGURE LEGENDS

Figure 1.

Spermidine expands lifespans of mice in a MPA1S-dependent way. (**A,B**) Immunoblot analyses (**A**) and quantification (**B**) of levels of MAP1S in liver tissues from 18-month-old wild-type or MAP1S$^{-/-}$ mice drinking normal (Ctrl) or spermidine-containing water (SPD). The relative levels of proteins including MAP1S and LC3-II shown here and later were always calculated against the levels of their respective β-Actin loading controls. Plots were the means ± S.D. of at least three mice and the significance of the differences were compared using Student's t test. (**C**) Comparative analyses of the levels of oxidative stress among liver tissues from 18-month-old wild-type or MAP1S$^{-/-}$ mice drinking normal or spermidine-containing water by staining with dihydroethidine hydrochloride. Bar = 50 μm. (**D**) Plots of the relative levels of oxidative stress as shown in panel (**C**). (**E**) Comparative H&E staining among the liver tissues from mice described in (**A**). Bar = 20 μm. (**F**) Plots of the relative intensities of sinusoidal dilatation in liver tissues as described in (**E**). (**G**) The Kaplan-Meier survival curves showing the survival times of wild-type or MAP1S$^{-/-}$ male mice drinking normal or spermidine-containing water. (**H**) A table summarizing median survivals and hazard ratios based on the plots in (**G**). The significance of difference between two groups was estimated by log-rank test and p value for each plot was the probability larger than the χ^2 value.

Figure 2.

Spermidine alleviates CCl_4-induced mouse liver fibrosis in a MAP1S-dependent way. (**A**) Representative images of liver tissues from wild-type and MAP1S$^{-/-}$ mice untreated (Oil) or treated with CCl_4 (CCL4) and then subjected to drinking normal (Ctrl) or spermidine-containing water (SPD). (**B-D**) Plots of body weights (**B**), liver weights (**C**) and ratios of body weight to liver weight (**D**) of mice similarly treated as shown in panel (**A**). (**E**) Comparative H&E staining among the liver tissues from CCl_4-treated wild-type and MAP1S$^{-/-}$ mice drinking normal or spermidine-containing water. Bar = 10 μm. (**F**) Plots of the relative intensities of liver lesions in liver tissues as shown in (**E**). (**G**) Comparative Sirius Red staining among the liver tissues as described in (**E**). Bar = 10 μm. (**H**) Plots of the Sirius Red staining positive areas as shown in (**G**). (**I**) Plots of the levels of hydroxyproline in liver tissues as described in (**A**). (**J,K**) A representative immunoblot (**J**) and quantification (**K**) of lysates from the same liver tissues as described in (**A**). Lysates with the same amount of total proteins were subjected to immunoblot with antibody against MAP1S, α-SMA or β-Actin. (**L,M**) Immunostaining analyses (**L**) and quantification (**M**) of α-SMA in CCl_4-treated liver tissues as described in (**E**). Bar = 200 μm.

Figure 3

Spermidine suppresses the development of HCC in DEN-treated mice through MAP1S. (**A**) Representative images of liver tissues from DEN-treated wild-type and MAP1S$^{-/-}$ mice drinking normal (Ctrl) or spermidine-containing water (SPD). (**B-E**) Plots of body weights (**B**), liver weights (**C**), ratios of body weight to liver weight (**D**) and number of surface tumors of mice similarly treated as shown in panel (**A**). (**F**) A comparative H&E

staining of liver sections of DEN-treated 7-month-old mice as described in (**A**). Bar = 10 μm. (**G-I**) Immunoblot analyses (**G**) and quantification of the relative levels of MAP1S (**H**) and total poly-ubiquitinated proteins (**I**) in the normal liver tissues adjacent to tumor focus from 6 month-old mice as described in (**A**). (**J**) Representative immunostaining of γ-H2AX in liver sections of DEN-treated 7-month-old mice as described in (**A**). Bar = 10 μm. (**K**) A plot of percentage of γ-H2AX positive cells in total cells of liver tissues as described in (**J**).

Figure 4.

Spermidine promotes autophagy flux in a MPA1S-dependent way. (**A-D**) Immunoblot analyses (**A,C**) and quantification (**B,D**) of levels of MAP1S and LC3-II in MEF or HeLa cells treated with 100 μM spermidine (SPD) for different times (**A,B**) or different concentrations of spermidine for 4 hrs (**C,D**). The same amounts of total proteins were loaded in each lane and β-Actin serves as another loading control. (**E,F**) Immunoblot analyses (**E**) and quantification of LC3-II levels in HeLa cells treated with spermidine in the absence (None) or presence of bafilomycin A1 (BAF) (**F**). (**G,H**) Representative images (**G**) and quantification (**H**) of the number of RFP-LC3 punctate foci in HeLa cells stably expressing RFP-LC3 untreated (Ctrl) or treated with spermidine (SPD) in the absence (None) or presence of BAF. (**I,J**) Immunoblot analyses (**I**) and quantification (**J**) of LC3-II levels in organs collected from wild-type or MAP1S$^{-/-}$ mice untreated (-) or treated with spermidine (+). (**K,L**) Immunoblot analyses (**K**) and quantification (**L**) of LC3-II levels in MEF cells developed from wild-type or MAP1S$^{-/-}$ mice treated with different concentrations of spermidine. (**M,N**) Immunoblot analyses (**M**) and

quantification of (**N**) of LC3-II levels in hepatocytes isolated from wild-type or MAP1S$^{-/-}$ mice that were untreated or treated with spermidine in the absence or presence of BAF. (**O,P**) Immunoblot analyses (**O**) and quantification (**P**) of LC3-II levels in MEFs developed from wild-type or MAP1S$^{-/-}$ mice that were untreated (Ctrl) or treated with spermidine (SPD) in the absence or presence of BAF.

Figure 5.

Spermidine regulates subcellular distribution of HDAC4 to enhance acetylation and stability of MAP1S. (**A**) Immunoblot analyses of acetylated MAP1S in HeLa cells untreated (-) or treated with spermidine (+). Acetylated MAP1S was precipitated with antibody against MAP1S and visualized with antibody against acetyl lysine. (**B,C**) Immunoblot analyses (**B**) and quantification of levels of acetylated MAP1S (**C**) in HeLa cells untreated or treated with spermidine. Acetylated proteins were precipitated with agarose-conjugated antibody against acetyl lysine and visualized with antibody against MAP1S. (**D,E**) Immunoblot analyses (**D**) and quantification of levels of MAP1S in HeLa cells untreated or treated with spermidine at different times after protein translation was terminated with cycloheximide (CHX) (**E**). The values of t1/2 were the time required for half of MAP1S proteins to be degraded. (**F**) Immunoblot analysis of the co-immunoprecipitates of MAP1S and HDAC4 in HepG2 cells. (**G**) Immunoblot analyses of the impact of spermidine on levels of MAP1S and LC3 in HeLa cells treated with random (Mock) or HDAC4-specific siRNAs (HDAC4) in the absence or presence of BAF. (**H,I**) Plots of relative levels of MAP1S (**H**) and LC3-II (**I**) as shown in (**G**). (**J-N**) Immunoblot analyses of HDAC4 levels in HeLa cells treated with different concentration

of spermidine for 4 hrs (**J**) or 100 μM spermidine for different times (**K**), in MEF cells treated with different concentration of spermidine for 4 hrs (**L**), or in organs from 3 pairs of wild-type mice intraperitoneally injected with either saline or spermidine at a dosage of 50 mg/kg body weight (**M,N**). The relative levels of HDAC4 in representative images (**M**) are quantified (**N**). (**O,P**) Fluorescent microscopic analyses (**O**) and quantification (**P**) of the impact of spermidine on the distribution of GFP or GFP-HDAC4 in HeLa cells. (**Q,R**) Fluorescent microscopic analyses (**Q**) and quantification (**R**) of the impact of spermidine on the distribution of GFP-HDAC4 in wild-type MEF cells. (**S,T**) Immunoblot analyses (**S**) and quantification (**T**) of the impact of spermidine on the distribution of HDAC4 in different subcellular fractions of HeLa cells.

Figure 6.

Spermidine reduces the chances of HDAC4 forming complex with MAP1S. (**A,B**) Immunoblot analyses (**A**) and quantification (**B**) of the impact of spermidine on the levels of total or phosphorylated HDAC4 or 14-3-3. (**C,D**) Immunoblot analyses (**C**) and quantification (**D**) of the impact of spermidine on the interaction between HDAC4 and 14-3-3. (**E-J**) Immunoblot analyses (**E,G,I**) and quantification (**F,H,J**) of the impact of spermidine on the interaction between HDAC4 and MAP1S as detected by coimmunoprecipitation with antibody against MAP1S (**E-H**) or HDAC4 (**I,J**). Lysates were prepared from HeLa cells carrying endogenous proteins (**E,F**) or overexpressing MAP1S and HDAC4 (**G-J**). (**K,L**) Fluorescent microscopic analyses (**K**) and quantification of (**L**) of the colocalization between MAP1S and HDAC4.

Figure 7.

Lysine 520 of MAP1S is important for MAP1S to promote autophagosomal degradation. (**A**) Coimmunoprecipitation analyses of the interaction of HDAC4 with wild-type (WT) or K520R mutant MAP1S in 293T cells transiently expressing wild-type or K520R mutant MAP1S. (**B**) Analyses of the colocalization of HDAC4 with wild-type and K520R mutant MAP1S. (**C-F**) Analyses of the impact of K520R mutation on autophagy flux. Representative immunoblots of LC3-II in HeLa cells (**C**) and fluorescent microscopic images of RFP-LC3 punctate foci in HeLa cells stably expressing RFP-LC3 (**E**) and their respective quantification (**D,F**) are shown. (**G,H**) Analyses of the impact of K520R mutation on the colocalization of RFP-LC3 punctate foci with lysosomes stained with anti-LAMP2 antibody. Representative images (**G**) show lysosome-associated (yellow in merge) and lysosome-free RFP-LC3 punctate foci (red spots, some are pointed out using white arrows). Quantification (**H**) shows the percentages of lysosome-free to total RFP-LC3 punctate foci. (**I,J**) Analyses of the impact of K520R mutation on the ability for MAP1S to restore the impact of spermidine on autophagy flux in MAP1S$^{-/-}$ MEFs. Representative immunoblots (**I**) and quantification (**J**) are shown.

Author Manuscript Published OnlineFirst on April 6, 2017; DOI: 10.1158/0008-5472.CAN-16-3462
Author manuscripts have been peer reviewed and accepted for publication but have not yet been edited.

Figure 1

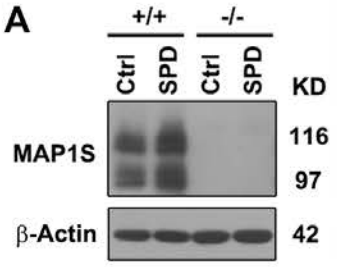

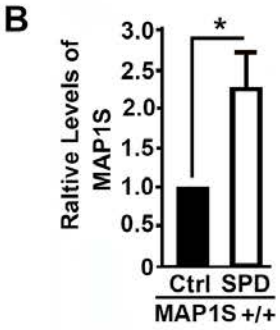

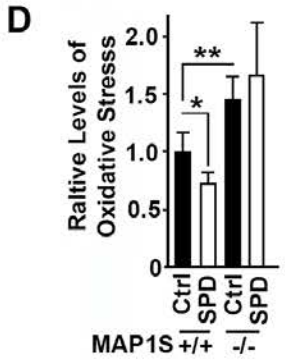

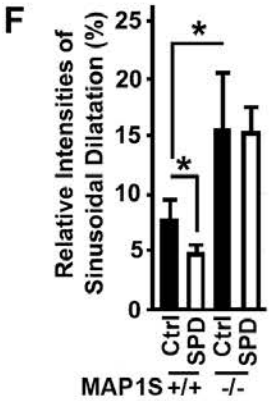

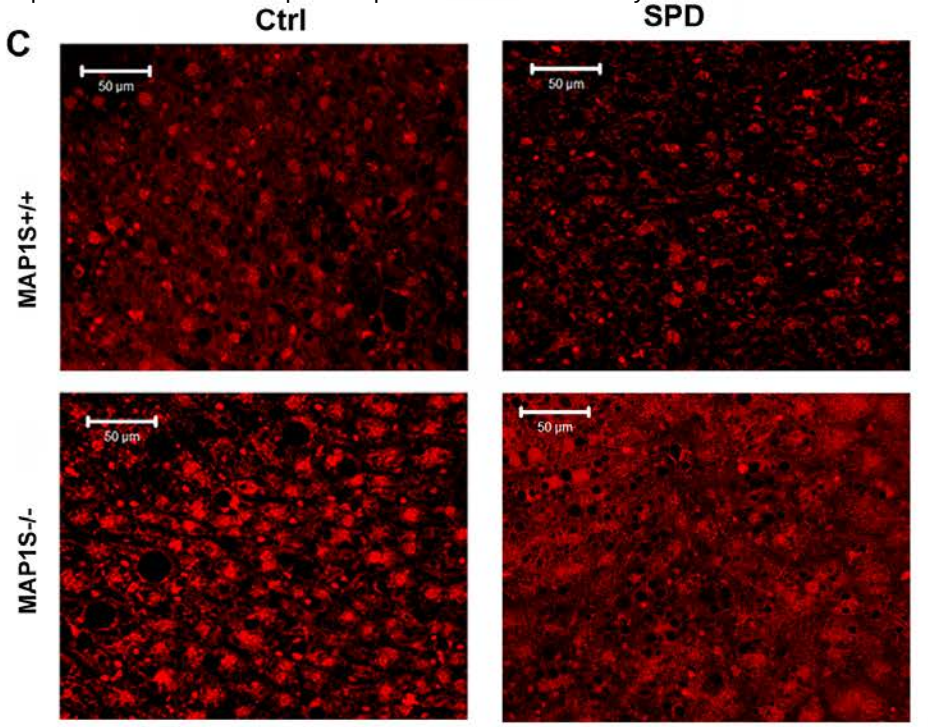

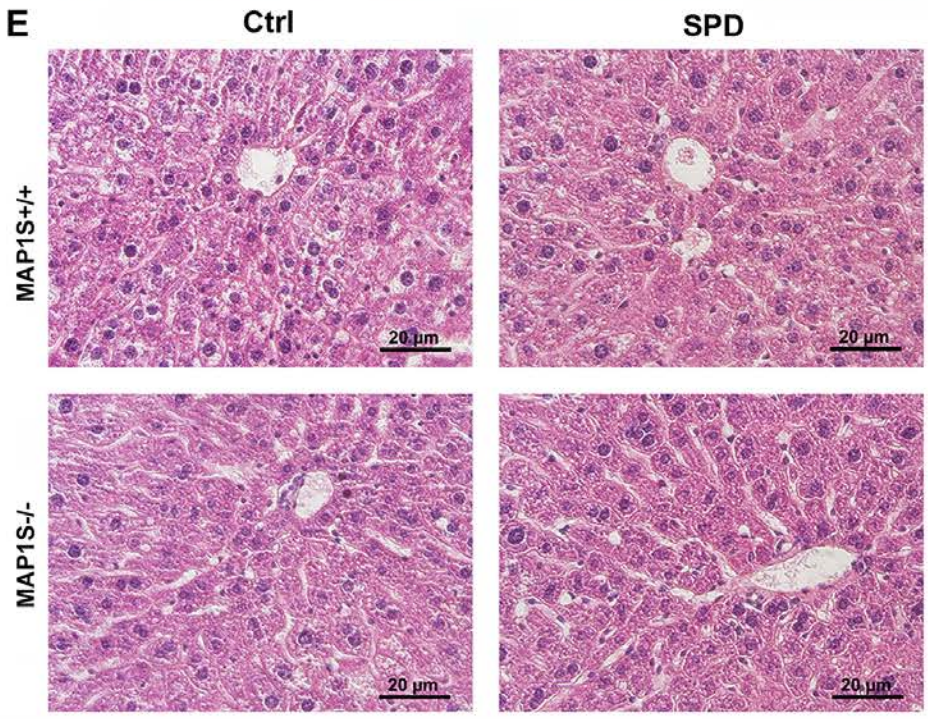

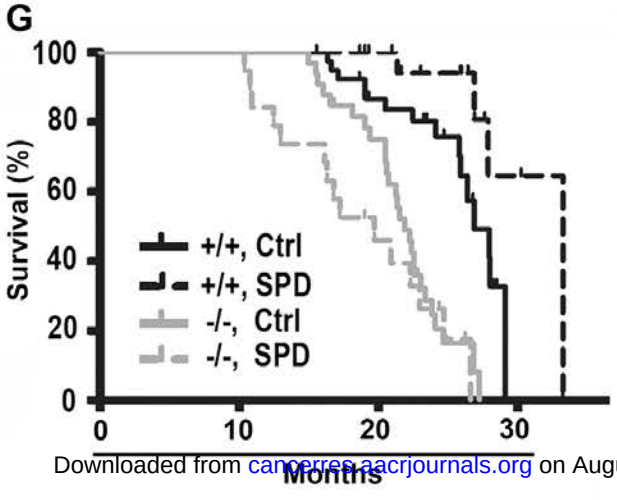

H

Median Survival and Hazard Ratio (HR)

	Number of Mice	Median Survival (Months)	+/+ Ctrl	+/+ SPD	-/- Ctrl
+/+ Ctrl	40	26.9			
+/+ SPD	22	33.3	3.08$^{\alpha}$ 1.19-7.99$^{\beta}$ 0.020$^{\gamma}$		
-/- Ctrl	33	21.9	0.21$^{\alpha}$ 0.11-0.41$^{\beta}$ 0.000$^{\gamma}$	0.14$^{\alpha}$ 0.06-9.29$^{\beta}$ 0.000$^{\gamma}$	
-/- SPD	19	19.7	0.11$^{\alpha}$ 0.04-0.28$^{\beta}$ 0.000$^{\gamma}$	0.06$^{\alpha}$ 0.02-0.17$^{\beta}$ 0.000$^{\gamma}$	0.70$^{\alpha}$ 0.36-1.38$^{\beta}$ 0.090$^{\gamma}$

α, Hazard Ratio; β, 95% Confident Interval; and γ, P value.

Author Manuscript Published OnlineFirst on April 6, 2017; DOI: 10.1158/0008-5472.CAN-16-3462
Author manuscripts have been peer reviewed and accepted for publication but have not yet been edited.

Figure 2

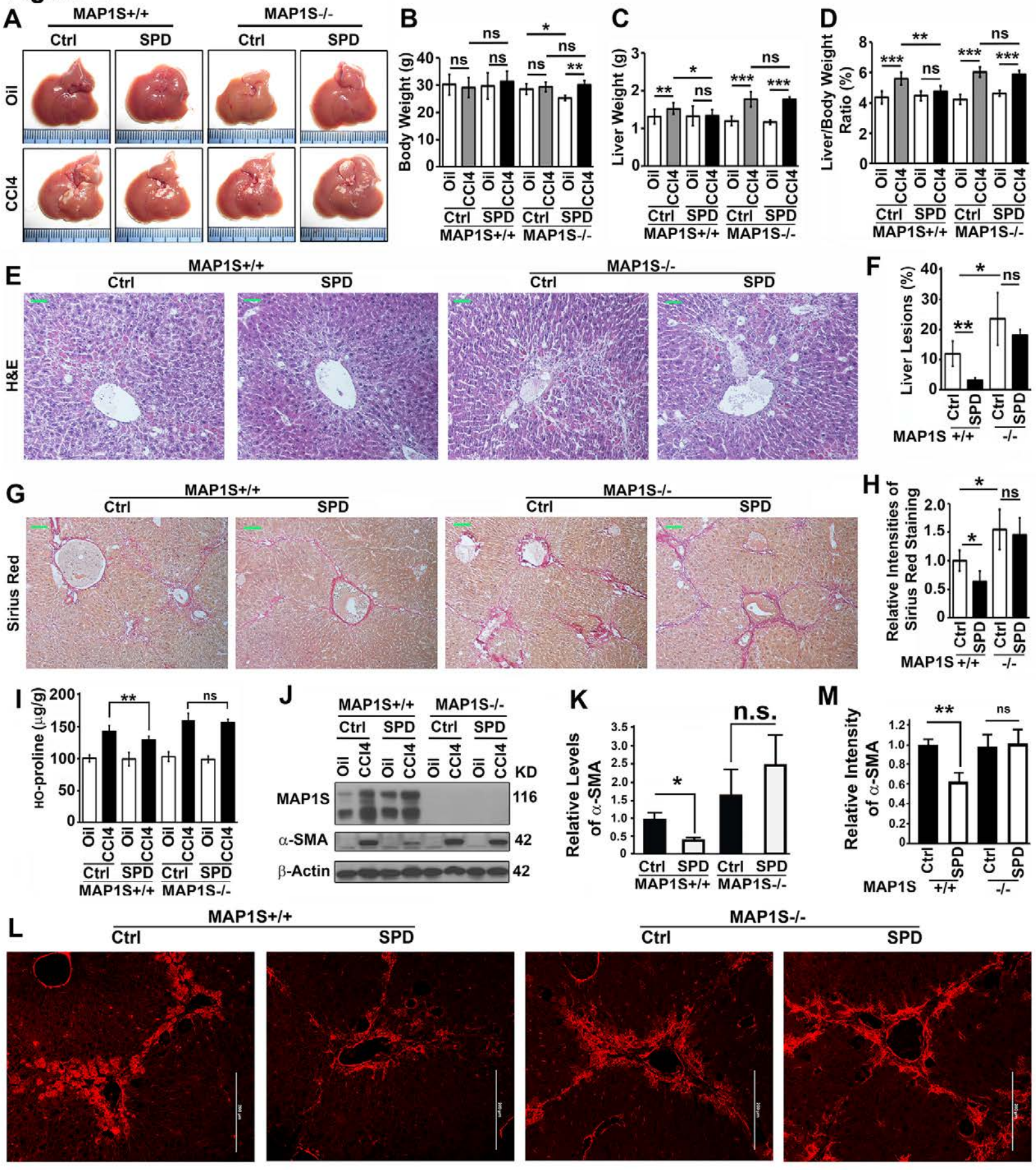

Figure 3

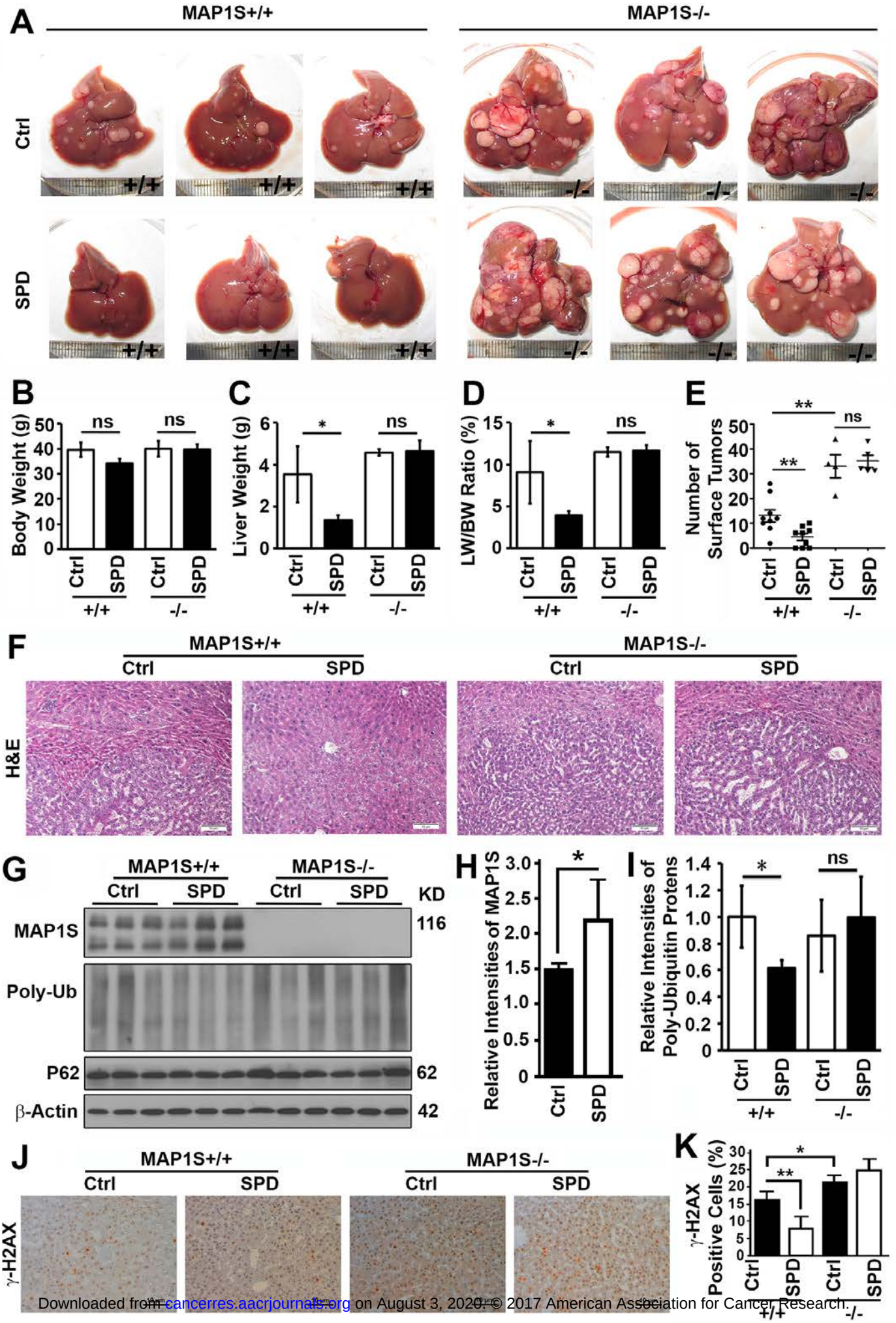

Author Manuscript Published OnlineFirst on April 6, 2017; DOI: 10.1158/0008-5472.CAN-16-3462
Author manuscripts have been peer reviewed and accepted for publication but have not yet been edited.

Figure 4

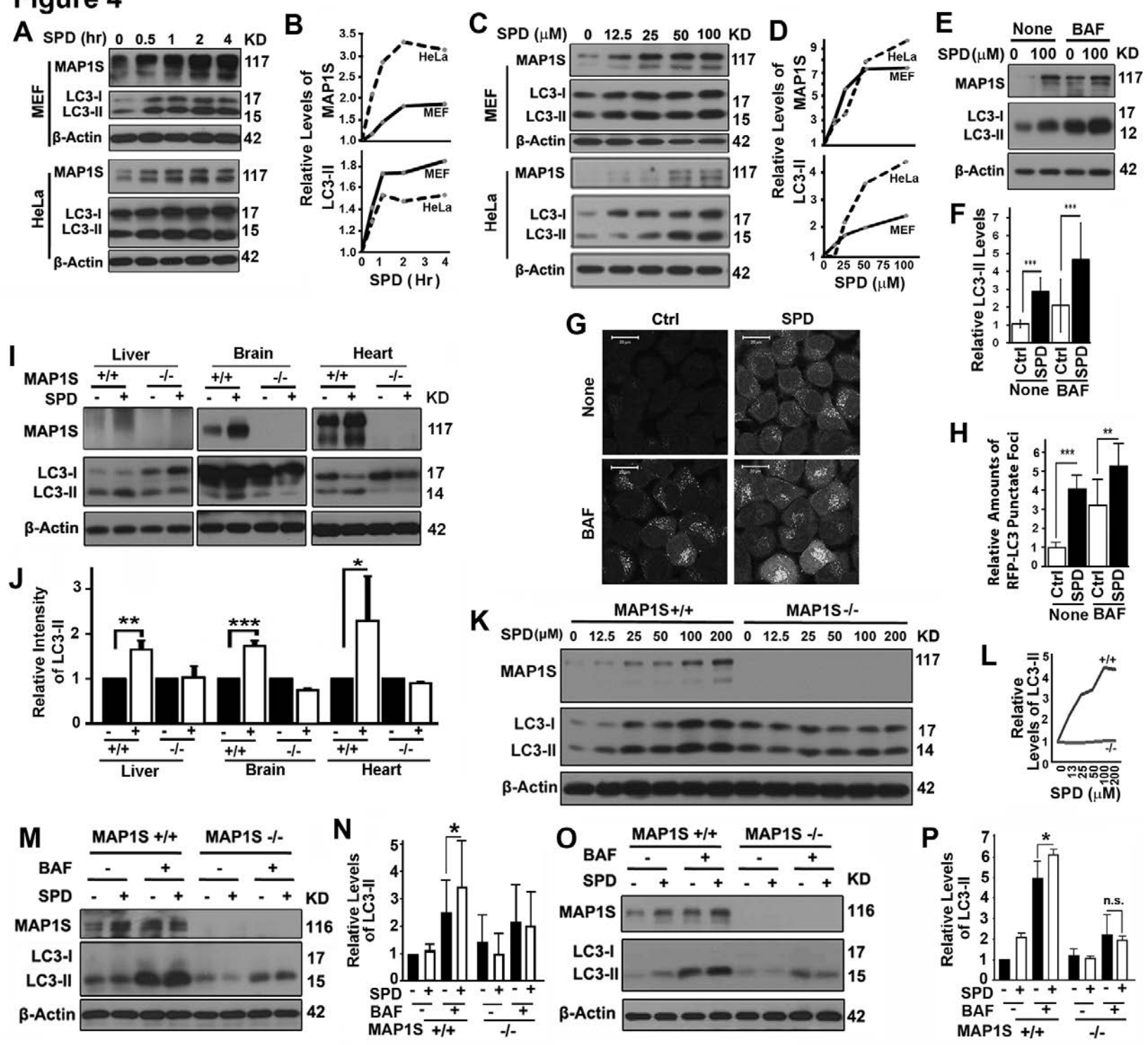

Figure 5

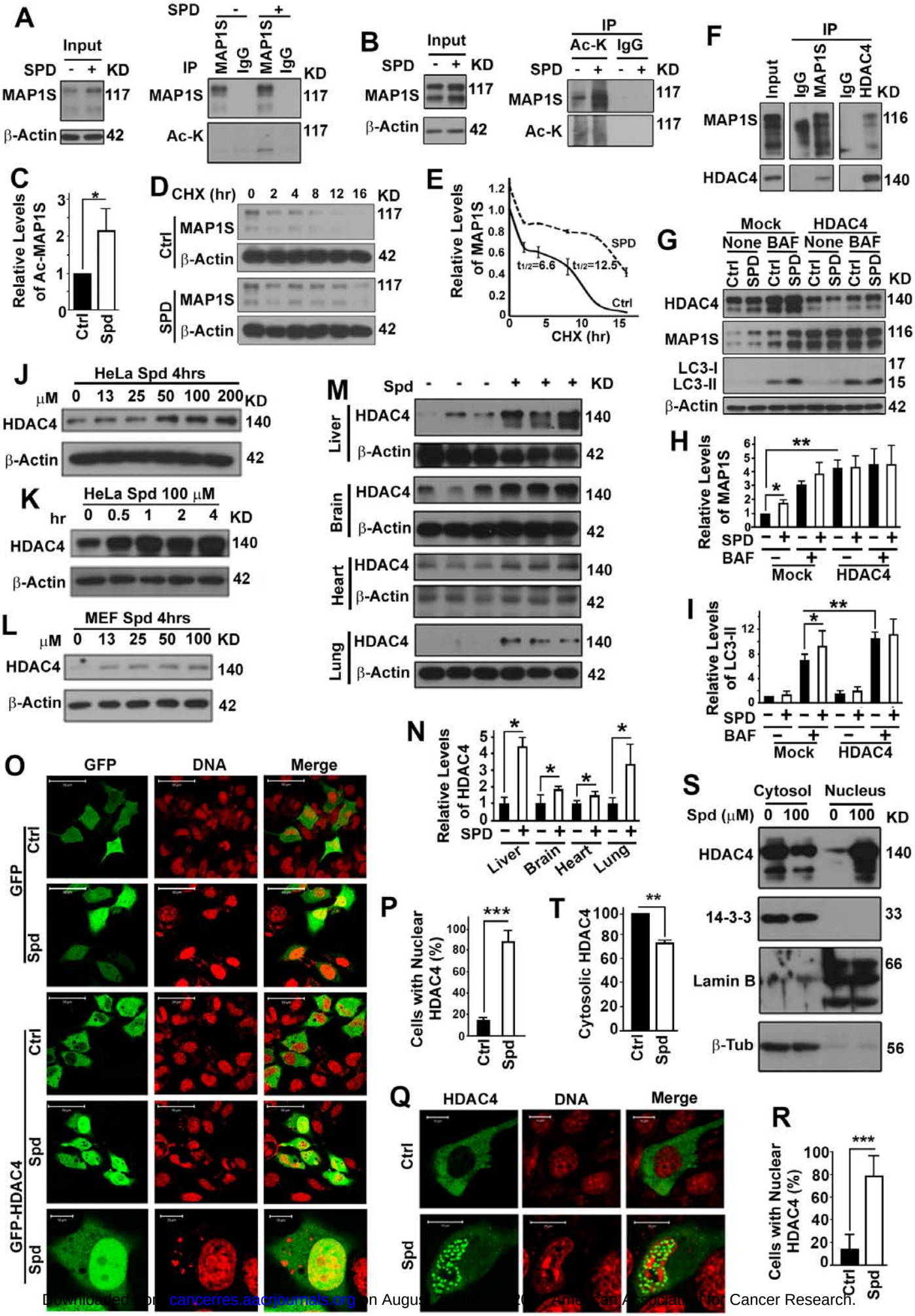

Figure 6

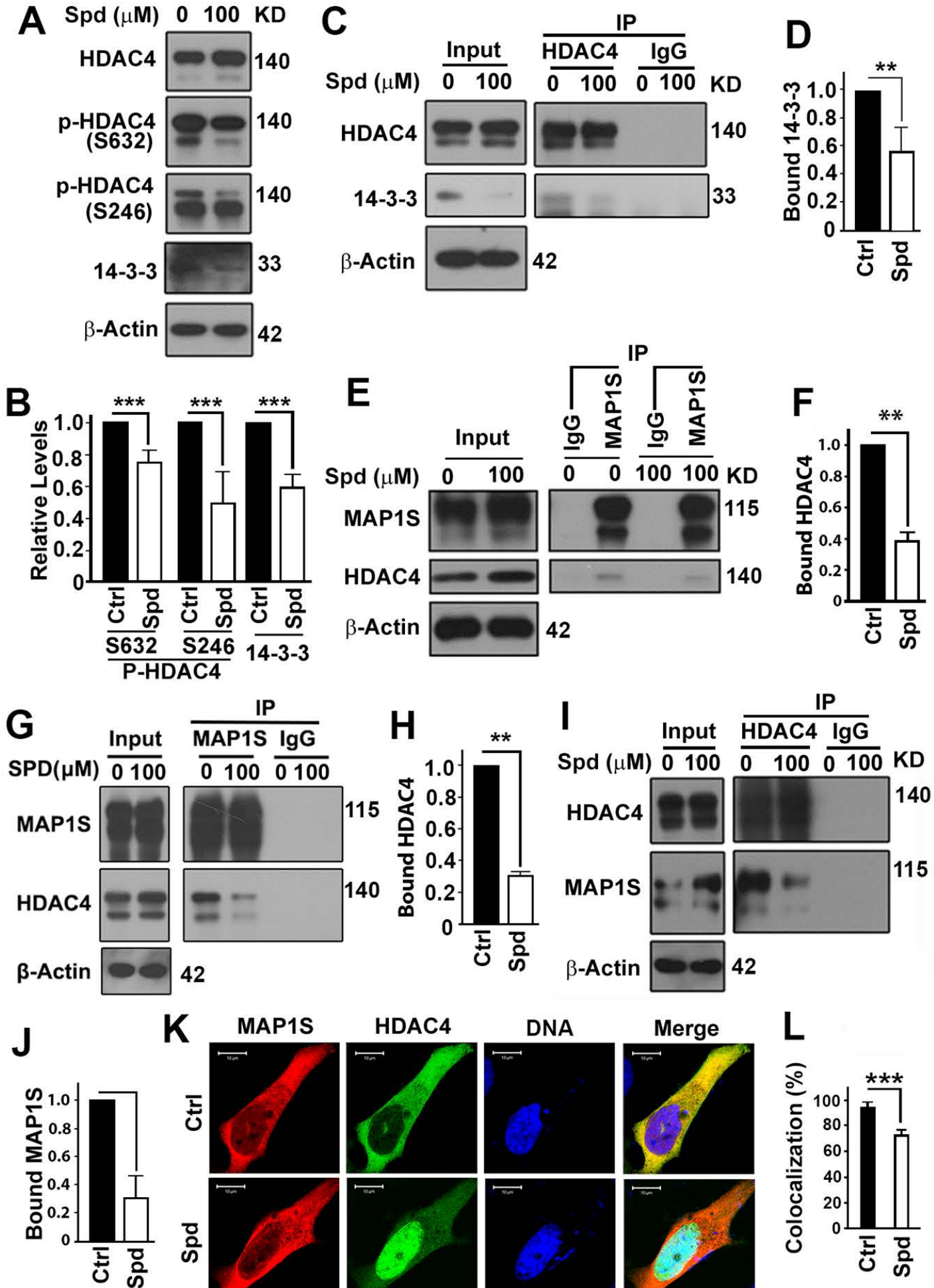

Author Manuscript Published OnlineFirst on April 6, 2017; DOI: 10.1158/0008-5472.CAN-16-3462
Author manuscripts have been peer reviewed and accepted for publication but have not yet been edited.

Figure 7